JACS
JOURNAL OF THE AMERICAN CHEMICAL SOCIETY
pubs.acs.org/JACS
Article

Periodic Superlattice Modulation of Monolayer Borophene by Adsorption of Boron Clusters

Chen Ma,[‡] Yunlei Wang,[‡] Xiaoshuang Li, Baojie Feng, Haifeng Lv,* Kehui Wu, Yeliang Wang, HongJun Gao, Xiaojun Wu,* and Lan Chen*

Cite This: J. Am. Chem. Soc. 2026, 148, 8276−8284
Read Online
ACCESS | Metrics & More | Article Recommendations | Supporting Information

ABSTRACT: Elemental boron exhibits remarkable polymorphism and strong substrate dependence in phase formation due to its intrinsic electron deficiency and highly delocalized bonding nature. These unique characteristics pose significant chance for the controlled synthesis of well-defined boron-based phases through substrates engineering. In this study, we demonstrate the structure modulation of monolayer borophene (MLB) with atomic precision by the adsorption of small boron clusters on Cu(100). Through combined scanning tunneling microscopy (STM) and first-principles calculations, we identify these small clusters as B_7 and reveal their non-close-packed selective adsorption behaviors, which templates the formation of distinct boron cluster chain configurations. The strong interfacial coupling between B_7 clusters and the MLB induces spontaneous migration of boron atoms from dislocation sites, leading to dynamic and periodic modulation of the boron superlattice in MLB. Our work establishes a novel paradigm for the bottom-up construction of low-dimensional boron phases and realizes the periodic superlattice modulation of MLB through adsorption of boron clusters, providing new insight into fabricating polymorphs of borophene beyond the choice of substrates.

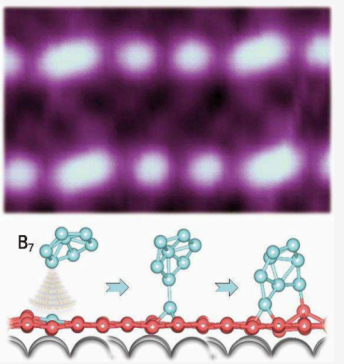

INTRODUCTION

The electron-deficient nature of boron drives its propensity for multicenter bonding through electron sharing, resulting in extensive electron delocalization. This unique bonding characteristic gives rise to a rich polymorphism in low-dimensional boron allotropes, manifesting as zero-dimensional (0D) magic-number clusters[1−7] and medium-sized boron core−shell structures,[8,9] one-dimensional (1D) nanoribbons and nanotubes,[10−12] and two-dimensional (2D) nanosheets such as borophene.[13−15] The resulting structural diversity endows boron with exceptional physical properties, including ultrahigh mechanical strength,[16,17] one-dimensional electron gas behavior,[18] plasmonic excitations,[19] and even superconductivity,[20−22] which have attracted significant research interests worldwide. However, the high chemical reactivity of boron presents formidable challenges for the controlled synthesis of these low-dimensional allotropes.

Photoelectron spectroscopy studies have revealed that small boron clusters tend to exhibit planar or quasi-planar configurations, in stark contrast to the icosahedral B_{12} unit characteristics of bulk boron.[13,23−26] Extended boron clusters are believed to be fundamental precursors to borophene.[13,27,28] Experimentally, various borophene polymorphs with different hole densities (η) on metal substrates such as Ag(111)/(110)/(100),[10,11,29−32] Cu(111)/(100),[33−36] Au(111),[37] Al(111),[38] and Ir(111)[39] have been successfully synthesized. However, the structural characteristics of borophene is critically constrained by the substrate commensurability.[40,41] Specifically, the long-range ordering in borophene polymorphs is controlled by lattice matching and interfacial charge transfer between borophene and substrate.[42] Thus, achieving superlattice modulation beyond substrate confinement is quite challenging. This substrate dependence, while useful for accessing certain phases, inherently limits our ability to tailor borophene's superlattice periodicity independently of the substrate's constraints. However, it has been theorized that introducing boron clusters or other boron-rich species onto a borophene layer could modulate the borophene lattice itself, potentially enabling in situ superlattice engineering beyond what the substrate alone dictates.[43] Recently, the periodic and uniform B_5 cluster is experimentally synthesized on the Cu(111) supported monolayer borophene.[6] Of particular interest is the unique-sized B_5 cluster acting as a precursor for bilayer formation: once the clusters saturate the specific adsorption sites on the MLB, a domino-like structural transition results in the formation of the second layer. But the clusters are tightly bound at their adsorption sites due to the direct boron−boron covalent bonding with the MLB, which imposes a constraint on further structural tuning of the substrate. Challenges still

Received: October 17, 2025
Revised: February 4, 2026
Accepted: February 6, 2026
Published: February 17, 2026

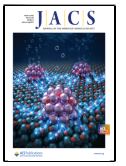

https://doi.org/10.1021/jacs.5c18362
J. Am. Chem. Soc. 2026, 148, 8276−8284

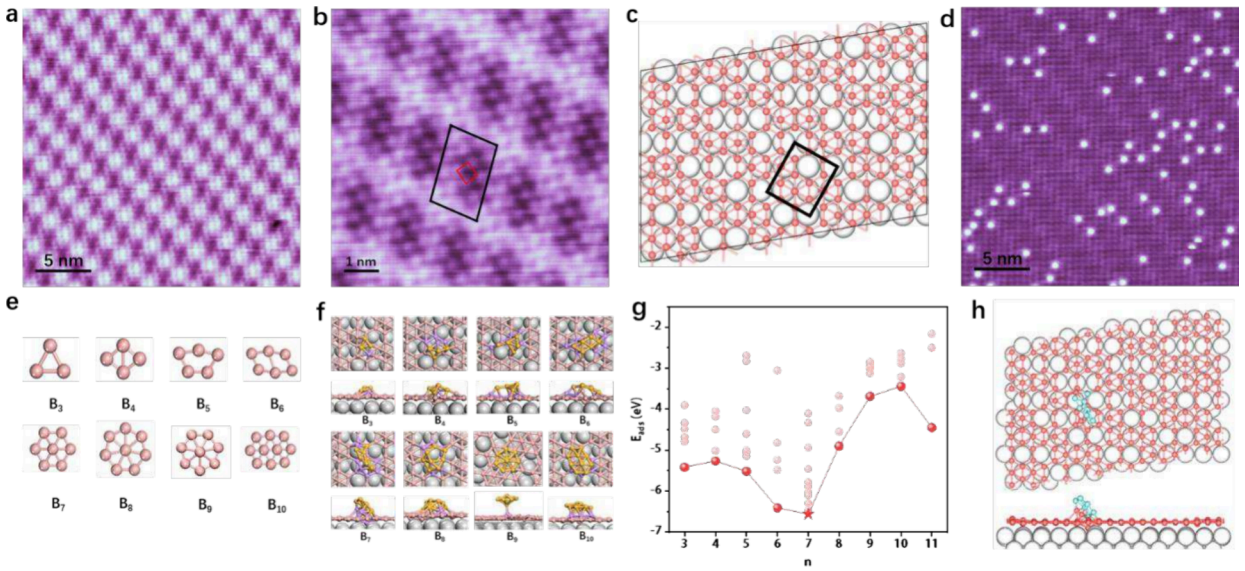

Figure 1. (a) STM image of MLB on a Cu(100) surface (scanning set point: I = 300 pA, V_{tip} = −3.5 V). (b) High-resolution STM image of MLB (scanning set point: I = 100 pA, V_{tip} = −1.06 V). The red rectangle and black parallelogram indicate the basic small unit cell and the large cell of the supermodulation, respectively. (c) Top view of structural model of MLB. The small pink and big gray spheres represent the boron and copper atoms, respectively. (d) STM images of boron clusters adsorbed on MLB (scanning set point: I = 100 pA, V_{tip} = 1.2 V). (e) Summary of the minimum-energy structures of B_n (n = 3 to 10) clusters resulting from theoretical studies. (f) Top view (top) and side view (bottom) of calculated structural models of B_n (n = 3 to 10) clusters adsorbed on MLB on Cu(100). The small pink and big gray spheres represent the boron atoms in MLB and copper atoms in Cu(100) substrate, respectively. The boron clusters are shown in yellow. Spheres in purple indicate boron atoms pulled up from MLB by interaction with boron clusters. (g) Adsorption energies of boron clusters per cluster, where n is the number of boron atoms in one boron cluster. (h) Top view (top) and side view (bottom) of structural model of MLB adsorbed with one B_7 cluster. The B_7 cluster is shown in blue.

remain in accurately predicting and experimentally verifying the optimal substrate−cluster interactions required for such precise superlattice engineering.

In this work, we successfully achieve periodic modulation of the MLB/Cu(100) superlattice by depositing boron clusters. Scanning tunneling microscopy (STM) reveals a nonclose-packed, preferential adsorption geometry for these clusters that templates the formation of diverse 1D boron chain structures. Especially, the strong cluster-MLB interaction drives boron atoms from the borophene's intrinsic dislocation sites to hop concertedly into adjacent vacant sites, leading to the unique lattice extension and periodic modulating the boron superlattice in MLB. Complementary charge and symmetry analyses (supported by first-principles calculations) confirm the emergence of interval-locked chain configurations. Below, we present these findings in detail, combining experimental observations with theoretical insights to elucidate the cluster−borophene interactions that drive the superlattice modulation.

RESULTS AND DISCUSSION

Characterization of MLB and Boron Clusters on MLB

The MLB was synthesized by depositing boron atoms on a clean Cu(100) surface, keeping the substrate temperature at 550 K. Figure 1a shows a large-area STM topography of the MLB on Cu(100). High-resolution STM in Figure 1b reveals MLB adopts a rectangle β_{13} phase with a unit-cell measuring 5.3 Å × 6.0 Å (outlined by the red rectangle), and a long-range supermodulation is observed (black parallelogram), forming a larger parallelogram superlattice with lattice parameters a = 30.7 Å, b = 20.2 Å, and γ = 80.5°, in excellent agreement with prior work. The atomic arrangement of the MLB on Cu(100) is shown in Figure 1c, indicating a hexagonal hole density η = 1/6 within the outlined region.[36] Upon complete coverage of the Cu(100) surface by the MLB, further boron deposition leads to the emergence of identical bright spots on the MLB (Figure 1d), analogous to previous observations for MLB on Cu(111), where extra boron also yields bright protrusions. In our case, each spot has a lateral size of 6.5 ± 0.3 Å and a height of 110 ± 10 pm, indicating the formation of boron clusters with identical sizes and geometry.

To determine the precise atomic structures of the boron clusters corresponding to these identical spots at low boron coverage, we performed density functional theory (DFT) simulations by placing boron clusters B_n (n = 3−18)[14,23,44−46] (Figures 1e and S2) within the β_{13} unit cell of the MLB at plausible adsorption sites. The relaxed adsorption structures (Figures 1f and S3) show that among the clusters tested the B_7 cluster exhibits the strongest binding to MLB, with an adsorption energy of −6.561 eV per cluster with reference to the chemical potential of the boron cluster (Figures 1g and S4) and −5.889 eV per cluster with reference to the chemical potential of a single boron atom or boron atom in the bulk phase (Figure S5), preferring to be a potential nucleation seed. In its most stable adsorbed configuration, the B_7 cluster deforms into puckered, ribbon-like fragments and adsorbs vertically on the MLB (Figure 1h). Notably, driven by the strong B_7−MLB interaction, two boron atoms from the MLB substrate pulled out and incorporated into the B_7 cluster, forming a B_9^- cluster anchored to the surface (Figure S6a). The formation of the anionic B_9^- cluster is attributed to preferential adsorption of B_7 cluster on the electron-rich boron atoms in MLB, which is further validated by the joint Bader charge analysis (Figure S7). Further, a multicenter bonding analysis supports the exceptional stability of the B_7-derived

https://doi.org/10.1021/jacs.5c18362
J. Am. Chem. Soc. 2026, 148, 8276−8284

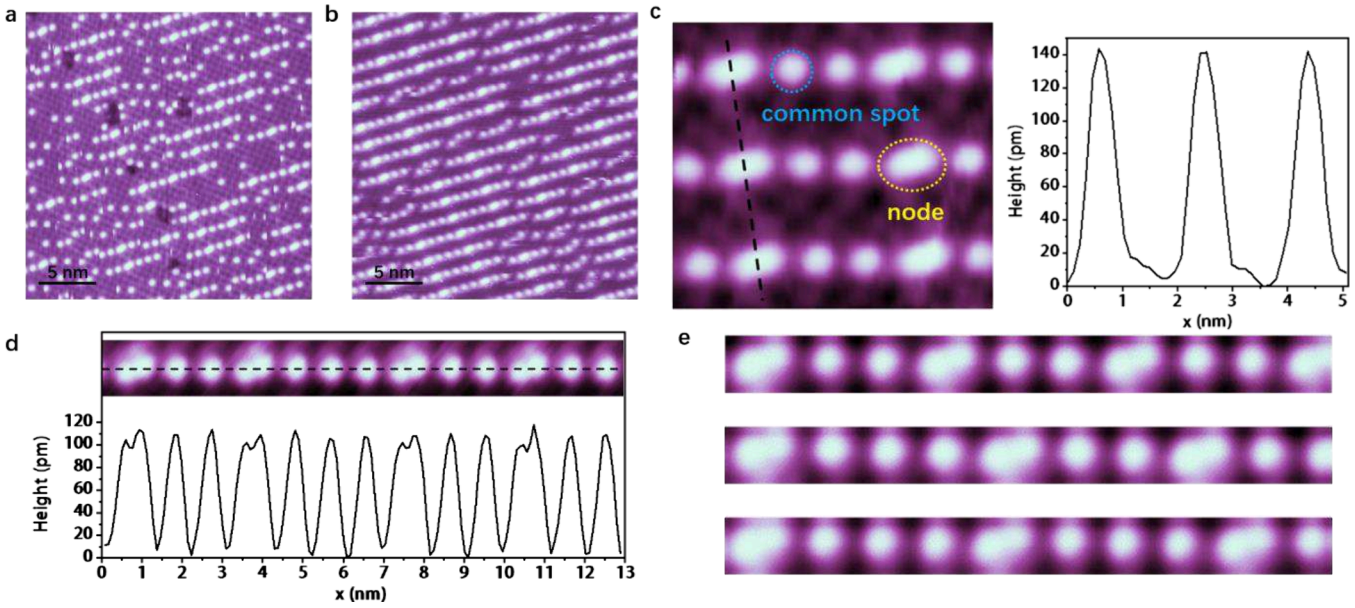

Figure 2. (a, b) STM images of ordered boron clusters adsorbed on MLB with increasing coverage of boron clusters (scanning set point: (a) I = 50 pA, V_{tip} = 1.3 V; (b) I = 100 pA, V_{tip} = −1.2 V). (c) (Left) High-resolution STM image of the ordered boron chain-like structure on MLB (scanning set point: I = 50 pA, V_{tip} = 1.3 V) and (right) height profile along the black dash line in (c). (d) Height profile of the ordered boron structure on MLB along the black dash line in inset. (e) High-resolution STM images of different modes of chain-like boron structure: (top) 2-mode; (middle) mixed-mode; (bottom) 3-mode. (scanning set point: I = 50 pA, V_{tip} = 2.3 V).

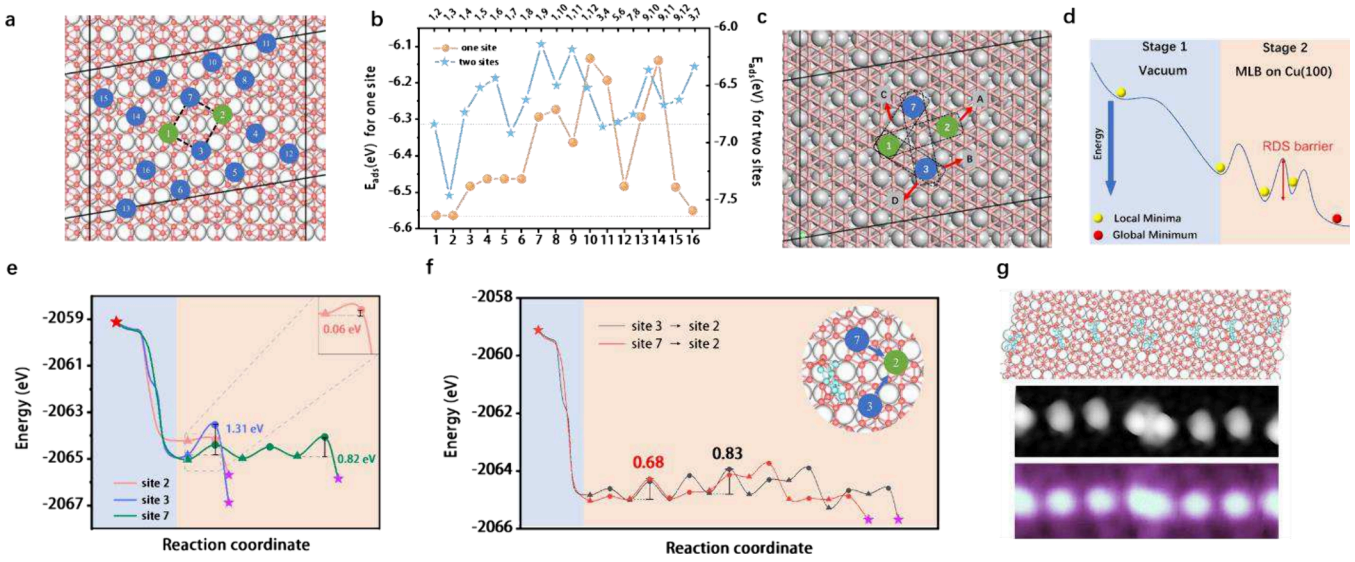

Figure 3. (a) Adsorption sites (labeled by numbers 1 to 16) in the unit cell of MLB on Cu(100). The green circles labeled with numbers 1 and 2 correspond to the experimental adsorption sites of the ordered boron structure within the unit cell of MLB on Cu(100). (b) Adsorption energies per cluster of one and two B_7 clusters on different sites. (c) Four combinations of adsorption sites for two B_7 clusters within the unit cell of MLB on Cu(100), labeled from A to D, respectively. (d) Schematic diagram for potential energy surface of boron cluster adsorption on MLB. (e) Minimum energy pathways during the adsorption of the second B_7 cluster, from vacuum to site 2,3,7 on MLB, corresponding to (c). The inset shows the highest RDS barrier for adsorption to site 2. (f) Energy pathways during the migration of the second B_7 cluster from site 3 to site 2 and from site 7 to site 2, respectively. The inset shows diagram of the migration of clusters. (g) Top: Structural model of 2-mode ordered adsorption of B_7 clusters on MLB. Middle: Simulated STM image based on the structural model (g (top)). Bottom: Experimental STM image of 2-mode ordered adsorption of B_7 clusters on MLB. The simulated STM image shows very good agreement with the experimental result.

cluster (formed B_9^-) (Figure S6b), which possesses four 2c−2e σ bonds, seven 3c−2e σ bonds, three 4c−2e σ bonds, and one 5c−2e π bond with the occupation numbers between ON = 1.81 and 1.94 |e|. This theoretical result illustrates the exceptional binding strength of the B_7 cluster: the cluster not only covalently bonds to the borophene via B−B bonds but also scavenges nearby boron atoms, locally extending the borophene lattice into the third dimension (albeit by only a single atomic layer). In the experiments, the STM appearances of the clusters remained uniform, which suggests that this incorporation of two substrate boron atoms likely occurs consistently for each cluster or that the process stabilizes the cluster without creating distinguishable new features (the cluster plus two pulled atoms still appears as one "spot").

https://doi.org/10.1021/jacs.5c18362
J. Am. Chem. Soc. 2026, 148, 8276−8284

Regardless, identifying the cluster as B_7 was further supported by our simulated STM images and energy analyses, as discussed below.

1D Chain Structure Formed by Constrained Adsorption of B_7 Clusters

As the boron coverage increases, the identical bright spots gradually arrange into ordered, periodic 1D chain-like structures. Figure 2a,b shows STM images of the surface at intermediate and higher cluster coverages, respectively, where the formation of linear arrangements of clusters is evident. High-resolution STM images (Figure 2c) reveal that within each chain the bright features occur in two distinct forms: single isolated spots (which we term "common spot") and pairs of brighter, closely spaced spots (which we term "node"). Based on the number of common spots between adjacent nodes, the evolving 1D chain-like structures with increasing boron coverage can be classified into three distinct modes: a 2-mode chain consisting of a periodic sequence of two spots per interval (Figure 2e, top), a 3-mode chain with a periodic sequence of three spots per interval (Figure 2e, bottom), and a 2−3 mixed mode with alternating sequence of two and three spots (Figure 2e, middle). These modes represent different chain-ordering configurations of clusters, which evolve from 2-mode to mixed mode and finally to 3-mode as boron coverage increases. LEED (Figure S8a−d) and fast Fourier transform (FFT) analysis of the high-resolution STM images (Figure S8e,f) confirms that all chains are aligned with the long-axis of the MLB superlattice's large unit cell. Notably, regardless of the chain mode, the interspot spacing within chains and the interchain separation remain constant. Specifically, for the exemplar 2-mode chains, the measured intrachain node spacing (29.8 Å, Figure 2d) and interchain distance (19.7 Å, Figure 2c) closely match the lattice parameters of the MLB superlattice's large cell (30.7 Å × 20.2 Å, Figure 1b). This one-to-one correspondence strongly suggests that the 2D borophene superlattice serves as a template for the 1D chain structure. In essence, the position of the B_7 cluster (both common spots and nodes) is locked to the underlying periodic "grid" defined by the MLB's dislocation network. The constrained arrangement yields an interval-locked, highly ordered assembly of clusters that mirrors the intrinsic borophene lattice periodicity.

To further clarify the details of 2-mode chain structure on MLB, we turned to first-principles calculations to evaluate possible adsorption sites and cluster interactions. We first concentrated on the common spots (isolated single B_7 clusters). By systematically scanning 16 possible adsorption sites (labeled 1−16) within the MLB unit cell (Figure 3a) using DFT calculations, we determined the energy profile (Figure 3b), revealing that a single B_7 cluster preferentially adsorbs at site 1 and site 2 (green circle), with a maximum adsorption energy of −6.563 eV per cluster. The site 16 with second highest adsorption energy of −6.497 eV is ruled out since it owns lower stability than site 1 and site 2 (0.066 eV) and can hardly form the line-mode as observed in experiment. For two B_7 clusters absorbed simultaneously, the most stable configurations within the β_{13} unit cell are sites 1−2, 1−3, 1−7 (Figure 3c, labeled A, B, and C), which exhibit the highest adsorption energies. The site 3−4 (D in Figure 3c) is ruled out in the formation of a complete 2-mode structure because it does not correspond to any observed chain ordering. Notably, site 1−2 (A in Figure 3c) matches the experimentally observed orientation of the 2-mode chain. However, interestingly, site 1−3 (B in Figure 3c) and site 1−7 (C in Figure 3c) configurations are thermodynamically more stable than site 1−2 by 0.625 eV/cluster and 0.080 eV/cluster, respectively. Purely thermodynamically, one might expect the chain structure to favor site 1−3 or 1−7 arrangements (which do not directly correspond to the uniform 2-mode pattern). The absence of those configurations in the experiment hints at kinetic factors influencing the assembly, as we explored next.

We performed kinetics analysis to understand how the second B_7 cluster attaches to a unit cell already containing one cluster. Specifically, we simulated the process of a B_7 cluster coming from a vacuum and adsorbing onto MLB that already has a B_7 cluster at site 1, examining different target sites for the incoming cluster. As shown in Figure 3d, this process occurs through two distinct stages: stage 1 is the initial adsorption from vacuum onto the surface without a significant barrier (essentially a spontaneous capture by the surface potential), and stage 2 consists of the cluster relocating from its initial landing position into the final adsorption site, which involves overcoming one or more energy barrier as it nudges into the optimal binding configuration alongside the first cluster. The highest energy barrier encountered in this multistep relocation defines the rate-determining step (RDS) barrier for the second cluster adsorption. Analysis of minimum energy pathways (Figures 3e and S10) reveals striking differences in adsorption kinetics; adsorption at site 2 requires overcoming an extremely low RDS barrier of only 0.06 eV. In contrast, site 3/7 presents significantly higher RDS barriers of 1.31/0.82 eV, respectively. We further investigated intersite migration pathways (Figures 3f, S11, and S12), finding that migration from site 3/7 to site 2 requires overcoming a 0.83/0.68 eV barrier. Notably, the intersite migration barrier is lower than the respective RDS barriers for direct adsorption at sites 3 and 7, suggesting that even if a cluster initially lands on a less favorable site, it can still relocate to site 2 given sufficient thermal energy, effectively funneling the system into the experimentally observed 2-mode ordering. These results suggest that clusters preferentially occupy sites that are adjacent but not directly neighboring, avoiding close packing due to unfavorable energetics. This explains the absence of a close-packed arrangement of B_7 clusters on the MLB.

Then to determine the optimal node configuration, we systematically evaluated 16 candidate arrangements of two B_7 clusters within the periodic dislocation region of MLB, which is the area where two adjacent clusters (at a node) reside. We ensure that our trial configurations respected the lattice matching observed (i.e., the spacing and alignment consistent with the MLB super superlattice). The energy profile in Figure S13a reveals that the most stable configuration exhibits an adsorption energy of −7.510 eV per B_7 cluster, with the corresponding atomic structure displayed in Figure S13b. The adsorption behavior at the node closely resembles that of a single cluster with the two adsorbed B_7 clusters forming a covalent bond between them. Based on the node structure, we re-evaluated the adsorption energies of two B_7 clusters, as shown in Figure S14. The results indicate that the combinations of sites 1−2, 1−3, and 1−7 within the β_{13} unit-cell yield the three most favorable adsorption energies, consistent with the scenario where node adsorption was not considered. Notably, sites 3−4 and 5−6 exhibit lower stability than site 1−2 by 0.043 and 0.055 eV per B_7 cluster, respectively, leading to their exclusion in subsequent analysis. The optimized structure and simulated STM image of the 2-

https://doi.org/10.1021/jacs.5c18362
J. Am. Chem. Soc. 2026, 148, 8276−8284

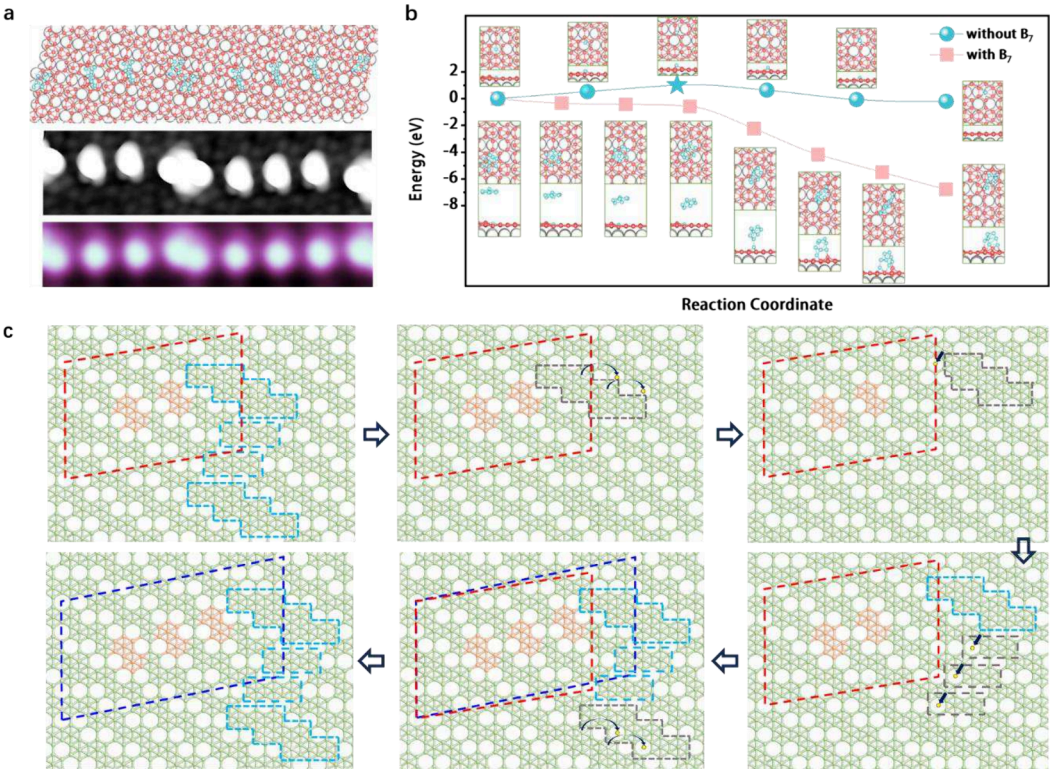

Figure 4. (a) Top: Structural model of mixed-mode ordered adsorption of B_7 clusters on extended MLB. Middle: Simulated STM image based on the structural model (a (top)). Bottom: Experimental STM image of mixed-mode ordered adsorption of B_7 clusters on extended MLB. (b) The potential energy pathway during the migration of a boron atom in the underlying MLB from its original site into the adjacent hole, induced by a B_7 cluster (marked in pink) or without a B_7 cluster (marked in cyan). The insets indicate different configurations during the migration. (c) Diagram of extension of the unit cell of MLB on Cu(100) with migration of boron atoms induced by B_7 clusters. MLB is shown in light green, and adsorption sites within the cell are shown in orange. The original cell and extended cell are marked by red parallelogram and dark blue parallelogram, respectively. Areas marked by light blue dash lines correspond to periodic dislocations in MLB. Areas marked by gray dash lines indicate those areas where migrations occur step by step.

mode ordered adsorption of B_7 clusters on MLB are presented in Figure 3g, which aligns well with the experimental observations for the 2-mode configuration.

Selective Modulation of the Borophene Structure

As the boron coverage increases, more complex structures (i.e., the 3-mode and the mixed-mode chains) emerge on a larger scale, but the interchain distance remains consistent with that of the 2-mode chains. Interestingly, within a single chain, three common spots exist between two adjacent nodes, resulting in an intrachain node distance of 38.3 Å, exhibiting a difference of 8.5 Å compared to the intrachain node distance (29.8 Å) in the 2-mode chains, which coincides with the spacing between two adjacent common spots. Therefore, due to the preferential adsorption sites from cluster−MLB interactions and observed chain ordering, we think the underlying borophene beneath the 3-mode and mixed-mode chains should undergo an anisotropic lattice expansion along the *a*-axis. Since the adsorption sites for nodes maintain strict registry with the periodic dislocations in the MLB superlattice, the extended superlattice should incorporate an additional unit cell of the β_{13} phase along the *a*-axis compared to the original structure. Thus, this expanded superlattice preserves the original adsorption sites for both common spots and nodes. For the 3-mode chains, the underlying structure consists of a continuously extended superlattice. In contrast, the mixed-mode chains should sit on expanded superlattices alternate with original superlattices along the *a*-axis. Consequently, all these structures keep a strict registry between the chains and the MLB.

The atomic structures of these extended MLB configurations are shown in Figure S15a,b, with optimized lattice constant extending to 38.6 and 69.4 Å, respectively. The adsorption energies of extended MLB on Cu(100) for 3-mode and mixed-mode are 0.025 and 0.018 eV/atom smaller than the original MLB (Table S1), respectively. Both configurations demonstrate an energetic stability. After adsorbing B_7 clusters, the adsorption energies of clusters on MLB are calculated to be −7.247 and −7.285 eV per cluster for 3-mode and mixed-mode, respectively (Table S2). The corresponding structural models are consistent with the experimental STM images (Figure S15c and Figure 4a).

The periodic extension of underlying MLB should be accompanied by migration of boron atoms on MLB. To delve into this process, we calculated the energetics of boron atom migration in the MLB induced by adsorbed B_7 cluster. Figure 4b plots the potential energy path for a single boron atom in the MLB hopping from its original site into a neighboring hexagonal hole. We compared two cases: with a nearby B_7 cluster (marked in pink) and without any cluster (cyan). The upper blue curve shows that the energy barrier of this migration without B_7 clusters is 1.03 eV. But the presence of B_7 clusters renders this process kinetically spontaneous. The inset illustrates representative atomic configurations along the migration pathway, indicating that B_7 adsorption actively pulls boron atoms from dislocation sites into new position

https://doi.org/10.1021/jacs.5c18362
J. Am. Chem. Soc. 2026, 148, 8276−8284

under the cluster and effectively extends the borophene lattice locally.

Figure 4c provides a schematic diagram of how these migrations extend the unit cell of MLB on Cu(100). The original MLB cell (red parallelogram) and the extended cell (dark blue parallelogram) are shown. Light green spheres denote the MLB lattice; orange spheres denote the preferred adsorption sites for B_7. Light blue dashed lines indicate the periodic dislocations in the MLB, and gray dashed lines mark the sequence of migration steps. In essence, each B_7 cluster induces a local expansion of the MLB lattice by pulling boron atoms from dislocation sites into its vicinity. When this effect is repeated periodically across the surface, that is, when many B_7 clusters adsorb at the regularly spaced dislocation sites, it produces the long-range superlattice modulation, as observed in our experiments. The boron chain motifs that become "locked" between clusters are a direct consequence of this anisotropic lattice expansion.

Here, we can understand this anisotropic lattice expansion process from a structural perspective. Within the boron superlattice, the hexagonal holes around each 6-fold coordinated boron atom are uniformly distributed, leading to randomly oriented hopping, averagely resulting in no net structural distortion, preserving the original configuration. However, in dislocation regions, the disparate hole distribution around 6-fold coordinated boron atom introduces directional preference in atomic hopping, leading to anisotropic lattice extension as experimentally observed. The B_7 clusters effectively trigger and guide this migration. In fact, B_7 clusters exhibit higher adsorption energy (per cluster) at sites along the dislocation lines than at other sites, indicating that the cluster-MLB interaction is strongest in those regions. This enhanced interaction is precisely what promotes the preferential pulling of boron atoms and the consequent lattice distortion there.

The distinct adsorption configuration of the B_7 cluster induces a periodic modulation of the MLB superlattice that would not occur on the bare substrate alone. This cluster-directed lattice engineering provides an effective strategy to overcome substrate-imposed constraints during borophene growth. By using adsorbed clusters to reshape the monolayer in situ, we achieve a new level of structural control: a periodically extended boron lattice with 1D chain incorporations that break the translational symmetry in a controlled fashion.

CONCLUSIONS

In summary, we successfully synthesized atomically small clusters in the B_7 size range on an MLB/Cu(100) surface, demonstrating their selective covalent attachment to MLB through B−B bonding to form 1D chain-like structures. With increasing boron coverage, we observed three distinct chain structure modes, all maintaining fixed interspot distances (between adjacent common spots) and consistent interchain spacing. Such distinct chain structures result from the directional and periodic modulation of the MLB superlattice through spontaneous concerted migration of boron atoms within adjacent hexagonal sites due to the strong B_7−MLB interaction. The detailed charge and symmetry analysis of MLB on Cu(100) reveals the site-dependent adsorption behavior, resulting in the formation of interval-locked chain structures. Our findings provide fundamental insights into cluster−substrate interactions, revealing boron's rich structural polymorphism while establishing a novel approach for controlled growth of substrate-supported borophene through cluster adsorption.

METHODS

Experimental Methods

The experiments were performed in an ultrahigh vacuum (UHV) MBE-STM system. The clean single-crystal Cu(100) substrate was prepared by repeated cycles of Ar^+ ion sputtering (with 2.5 keV energy at 2.0×10^{-5} Torr) and postannealing at ∼800 K. The growth of borophene and boron cluster was performed by evaporating pure boron (99.9999%), using a commercial electron-beam evaporator, onto the Cu(100) substrate in the MBE chamber with a base pressure of approximately 4.5×10^{-10} Torr. During boron growth, the Cu(100) substrate was kept at ∼550 K. The STM/scanning tunneling spectroscopy (STS) measurements were all performed at the liquid nitrogen temperature using a commercial Pt/Ir tip in the STM chamber (∼4.1×10^{-11} Torr). The WSxM software was used for image processing.

Calculation Details

We used density functional theory (DFT) combined with the projector augmented wave (PAW)[47,48] potential, as implemented in the Vienna *ab initio* simulation package (VASP),[49,50] for all calculations. The treatment of the exchange−correlation functional is within the generalized gradient approximation (GGA) using the Perdew−Burke−Ernzerhof (PBE) functional.[51] The energy cutoff of 500 eV is selected, and a Γ-centered Monkhorst−Pack k-point mesh featuring a k-space density of $2\pi \times 0.04$ Å^{-1} is employed. To prevent any unintended interactions, a vacuum spacing of 20 Å is set. The electronic self-consistent loop was converged to 10^{-6} eV and the convergence criteria for structure relaxations were set at 0.01 eV/Å, respectively. Dispersion corrections are included by the well-established Grimme's D3 method. The minimum energy paths are searched based on the climbing-image nudged elastic band (CI-NEB) method[52] with convergence criteria of 0.05 eV/Å for force. The structural models contain two Cu metal layers with the bottom layer fixed. The simulated STM image is obtained based on the Tersoff−Hamann theory and was visualized interfaced with the p4VASP package under the constant current mode.[53] The restricted B3LYP method and 6-31G(d,p) basis set are used to calculate the B_9^- boron clusters using the Gaussian 16 program.[54−56] The AdNAP analysis was plotted using the Multiwfn.[57] The first-principles molecular dynamics simulations are carried out at 550 K in the microcanonical ensemble with a time step of 1 fs.

The borophene layer was stretched and compressed to match the in-plane lattice constants of the underlying Cu(100) substrate. The Cu(100) lattice constant was kept fixed with lattice constant of (a = 30.7 Å, b = 20.2 Å, and γ = 80.5°). The specific borophene polymorph we studied has an equilibrium lattice constant of (a = 29.5 Å, b = 20.2 Å, and γ = 80.2°) when freestanding. When commensurated with the Cu(100) surface, it experiences a quasi-uniaxial strain of approximately 4.1% in the a direction.

To evaluate the thermodynamic stabilities of boron clusters on MLB, the average adsorption energy per cluster E_{ads} is defined as $[E_{tot} - (m{\cdot}E_{cluster} + E_{MLB} + E_{Cu})]/m$, where E_{tot} is the total energy of boron systems on Cu(100) substrate, $E_{cluster}$ is the energy of different boron cluster, E_{MLB} is the energy of different MLB, and E_{Cu} is the energy of Cu(100) substrate. m is the number of boron clusters in a large unit cell. To describe the interaction between boron systems and Cu(100) substrate, average adsorption energy per boron atom E'_{ads} is defined as $[E_{tot} - (E_{MLB} + E_{Cu})]/N_B$, where E_{tot} is total energy of boron systems on Cu(100) substrate, E_{MLB} is the energy of different MLB, and E_{Cu} is the energy of Cu(100) substrate. N_B is the number of boron atoms in a large unit cell. To calculate the adsorption energies of boron clusters on Cu(100) substrate with reference to the chemical potential of a single boron atom or boron atom in bulk boron, the average adsorption energy per boron atom is defined using the formula $E''_{ads} = [E_{tot} - (E_{MLB} + E_{Cu})]/N_B - E_{Boron}$, where E_{Boron} is the chemical potential of a single boron atom or boron atom in bulk boron, which

https://doi.org/10.1021/jacs.5c18362
J. Am. Chem. Soc. 2026, 148, 8276−8284

is a constant. The stability of free-standing borophene is characterized by the average energy per boron atom E_B, which is defined as E_{MLB}/N_B.

■ ASSOCIATED CONTENT

Supporting Information

The Supporting Information is available free of charge at https://pubs.acs.org/doi/10.1021/jacs.5c18362.

Additional experimental results about the MLB on Cu(100) with/without B_7 clusters absorbed (including STM image, LEED pattern, and FFT pattern), calculation results for the B_7 clusters and chain structure formed by constrained adsorption of these clusters, including adsorption energy curves of different configurations of boron clusters, electrostatic potential analysis, detailed charge analysis, and thermodynamic simulation (PDF)

■ AUTHOR INFORMATION

Corresponding Authors

Haifeng Lv − *State Key Laboratory of Precision and Intelligent Chemistry, School of Chemistry and Materials Science, and Collaborative Innovation Center of Chemistry for Energy Materials (iChEM), University of Science and Technology of China, Hefei, Anhui 230026, China;* orcid.org/0000-0001-9491-6367; Email: hflv@ustc.edu.cn

Xiaojun Wu − *State Key Laboratory of Precision and Intelligent Chemistry, School of Chemistry and Materials Science, and Collaborative Innovation Center of Chemistry for Energy Materials (iChEM), University of Science and Technology of China, Hefei, Anhui 230026, China; Hefei National Laboratory, University of Science and Technology of China, Hefei, Anhui 230088, China;* orcid.org/0000-0003-3606-1211; Email: xjwu@ustc.edu.cn

Lan Chen − *Institute of Physics, Chinese Academy of Sciences, Beijing 100190, China; School of Physical Sciences, University of Chinese Academy of Sciences, Beijing 100190, China;* orcid.org/0000-0003-4426-9944; Email: lchen@iphy.ac.cn

Authors

Chen Ma − *Institute of Physics, Chinese Academy of Sciences, Beijing 100190, China; School of Physical Sciences, University of Chinese Academy of Sciences, Beijing 100190, China*

Yunlei Wang − *State Key Laboratory of Precision and Intelligent Chemistry, School of Chemistry and Materials Science, and Collaborative Innovation Center of Chemistry for Energy Materials (iChEM), University of Science and Technology of China, Hefei, Anhui 230026, China*

Xiaoshuang Li − *Institute of Physics, Chinese Academy of Sciences, Beijing 100190, China; School of Physical Sciences, University of Chinese Academy of Sciences, Beijing 100190, China*

Baojie Feng − *Institute of Physics, Chinese Academy of Sciences, Beijing 100190, China; School of Physical Sciences, University of Chinese Academy of Sciences, Beijing 100190, China;* orcid.org/0000-0003-2332-7949

Kehui Wu − *Institute of Physics, Chinese Academy of Sciences, Beijing 100190, China; Tsientang Institute for Advanced Study, Zhejiang 310024, China*

Yeliang Wang − *MIIT Key Laboratory for Low-Dimensional Quantum Structure and Devices, School of Integrated Circuits and Electronics, Beijing Institute of Technology, Beijing 100081, China;* orcid.org/0000-0002-8896-0748

HongJun Gao − *Institute of Physics, Chinese Academy of Sciences, Beijing 100190, China; School of Physical Sciences, University of Chinese Academy of Sciences, Beijing 100190, China; Hefei National Laboratory, University of Science and Technology of China, Hefei, Anhui 230088, China;* orcid.org/0000-0002-6766-0623

Complete contact information is available at: https://pubs.acs.org/10.1021/jacs.5c18362

Author Contributions

‡C.M. and Y.W. contributed equally to this work.

Notes

The authors declare no competing financial interest.

■ ACKNOWLEDGMENTS

This work was financially supported by the Ministry of Science and Technology (MOST) of China (Grant 2024YFA1409100), the National Natural Science Foundation of China (Grants T2325028, 12134019, 22225301, 22303092), the Fundamental Research Funds for the Central Universities (Grants WK2490000001, WK2490000002, 20720250005), Quantum Science and Technology-National Science and Technology Major Project (Grant 2021ZD0303302), and Super Computer Centre of USTCSCC. L.C. acknowledges the support from the CAS Project for Young Scientists in Basic Research (Grant YSBR-054).

■ REFERENCES

(1) Zhai, H. J.; Kiran, B.; Li, J.; Wang, L. S. Hydrocarbon analogues of boron clusters-planarity, aromaticity and antiaromaticity. *Nat. Mater.* **2003**, *2* (12), 827−833.

(2) Gonzalez Szwacki, N.; Sadrzadeh, A.; Yakobson, B. I. B80 fullerene: an Ab initio prediction of geometry, stability, and electronic structure. *Phys. Rev. Lett.* **2007**, *98* (16), 166804.

(3) Jian, T.; Chen, X.; Li, S. D.; Boldyrev, A. I.; Li, J.; Wang, L. S. Probing the structures and bonding of size-selected boron and doped-boron clusters. *Chem. Soc. Rev.* **2019**, *48* (13), 3550−3591.

(4) Luo, X.-M.; Jian, T.; Cheng, L.-J.; Li, W.-L.; Chen, Q.; Li, R.; Zhai, H.-J.; Li, S.-D.; Boldyrev, A. I.; Li, J.; Wang, L.-S. B_{26}^-: The smallest planar boron cluster with a hexagonal vacancy and a complicated potential landscape. *Chem. Phys. Lett.* **2017**, *683*, 336−341.

(5) Wang, Y. J.; Zhao, Y. F.; Li, W. L.; Jian, T.; Chen, Q.; You, X. R.; Ou, T.; Zhao, X. Y.; Zhai, H. J.; Li, S. D.; Li, J.; Wang, L. S. Observation and characterization of the smallest borospherene, B_{28}^- and B_{28}. *J. Chem. Phys.* **2016**, *144* (6), 064307.

(6) Lv, H.; Chen, C.; Li, W.; Zhuo, Z.; Cheng, P.; Zhang, Y. Q.; Feng, B.; Wu, K.; Wu, X.; Chen, L. Selective binding and periodic arrangement of magic boron clusters on monolayer borophene. *Proc. Natl. Acad. Sci. U. S. A.* **2023**, *120* (11), No. e2215131120.

(7) Alexandrova, A. N.; Boldyrev, A. I.; Zhai, H.-J.; Wang, L.-S. Electronic Structure, Isomerism, and Chemical Bonding in B_7^- and B_7. *J. Phys. Chem. A* **2004**, *108* (16), 3509−3517.

(8) Zhao, J.; Wang, L.; Li, F.; Chen, Z. B_{80} and Other Medium-Sized Boron Clusters: Core-Shell Structures, Not Hollow Cages. *J. Phys. Chem. A* **2010**, *114* (37), 9969−9972.

(9) Li, F.; Jin, P.; Jiang, D.-e.; Wang, L.; Zhang, S. B.; Zhao, J.; Chen, Z. B_{80} and $B_{101-103}$ clusters: Remarkable stability of the core-shell

structures established by validated density functionals. *J. Chem. Phys.* **2012**, *136* (7), 074302.
(10) Zhong, Q.; Kong, L.; Gou, J.; Li, W.; Sheng, S.; Yang, S.; Cheng, P.; Li, H.; Wu, K.; Chen, L. Synthesis of borophene nanoribbons on Ag(110) surface. *Phys. Rev. Mater.* **2017**, *1* (2), 021001.
(11) Wang, Y.; Kong, L.; Chen, C.; Cheng, P.; Feng, B.; Wu, K.; Chen, L. Realization of Regular-Mixed Quasi-1D Borophene Chains with Long-Range Order. *Adv. Mater.* **2020**, *32* (48), No. e2005128.
(12) Kiran, B.; Bulusu, S.; Zhai, H.-J.; Yoo, S.; Zeng, X. C.; Wang, L.-S. Planar-to-tubular structural transition in boron clusters: B_{20} as the embryo of single-walled boron nanotubes. *Proc. Natl. Acad. Sci. U. S. A.* **2005**, *102* (4), 961−964.
(13) Piazza, Z. A.; Hu, H. S.; Li, W. L.; Zhao, Y. F.; Li, J.; Wang, L. S. Planar hexagonal B_{36} as a potential basis for extended single-atom layer boron sheets. *Nat. Commun.* **2014**, *5*, 3113.
(14) Li, W.-L.; Chen, X.; Jian, T.; Chen, T.-T.; Li, J.; Wang, L.-S. From planar boron clusters to borophenes and metalloborophenes. *Nat. Rev. Chem.* **2017**, *1* (10), 0071.
(15) Mannix, A. J.; Zhang, Z.; Guisinger, N. P.; Yakobson, B. I.; Hersam, M. C. Borophene as a prototype for synthetic 2D materials development. *Nat. Nanotechnol.* **2018**, *13* (6), 444−450.
(16) Zhang, Z.; Yang, Y.; Penev, E. S.; Yakobson, B. I. Elasticity, Flexibility, and Ideal Strength of Borophenes. *Adv. Funct. Mater.* **2017**, *27* (9), 1605059.
(17) Evans, M. H.; Joannopoulos, J. D.; Pantelides, S. T. Electronic and mechanical properties of planar and tubular boron structures. *Phys. Rev. B* **2005**, *72* (4), 045434.
(18) Kong, L.; Liu, L.; Chen, L.; Zhong, Q.; Cheng, P.; Li, H.; Zhang, Z.; Wu, K. One-dimensional nearly free electron states in borophene. *Nanoscale* **2019**, *11* (33), 15605−15611.
(19) Huang, Y.; Shirodkar, S. N.; Yakobson, B. I. Two-Dimensional Boron Polymorphs for Visible Range Plasmonics: A First-Principles Exploration. *J. Am. Chem. Soc.* **2017**, *139* (47), 17181−17185.
(20) Cheng, C.; Sun, J.-T.; Liu, H.; Fu, H.-X.; Zhang, J.; Chen, X.-R.; Meng, S. Suppressed superconductivity in substrate-supported β_{12} borophene by tensile strain and electron doping. *2D Mater.* **2017**, *4* (2), 025032.
(21) Gao, M.; Li, Q.-Z.; Yan, X.-W.; Wang, J. Prediction of phonon-mediated superconductivity in borophene. *Phys. Rev. B* **2017**, *95* (2), 024505.
(22) Penev, E. S.; Kutana, A.; Yakobson, B. I. Can Two-Dimensional Boron Superconduct? *Nano Lett.* **2016**, *16* (4), 2522−2526.
(23) Wang, L.-S. Photoelectron spectroscopy of size-selected boron clusters: from planar structures to borophenes and borospherenes. *Int. Rev. Phys. Chem.* **2016**, *35* (1), 69−142.
(24) Kawai, R.; Weare, J. H. Instability of the B_{12} icosahedral cluster: Rearrangement to a lower energy structure. *J. Chem. Phys.* **1991**, *95* (2), 1151−1159.
(25) Shirai, K. Phase diagram of boron crystals. *Jpn. J. Apl. Phys.* **2017**, *56* (5S3), 05FA06.
(26) Sun, X.; Liu, X.; Yin, J.; Yu, J.; Li, Y.; Hang, Y.; Zhou, X.; Yu, M.; Li, J.; Tai, G.; Guo, W. Two-Dimensional Boron Crystals: Structural Stability, Tunable Properties, Fabrications and Applications. *Adv. Funct. Mater.* **2017**, *27* (19), 1603300.
(27) Sadrzadeh, A.; Pupysheva, O. V.; Singh, A. K.; Yakobson, B. I. The Boron Buckyball and Its Precursors: An Electronic Structure Study. *J. Phys. Chem. A* **2008**, *112* (51), 13679−13683.
(28) Alexandrova, A. N.; Boldyrev, A. I.; Zhai, H.-J.; Wang, L.-S. All-boron aromatic clusters as potential new inorganic ligands and building blocks in chemistry. *Coord. Chem. Rev.* **2006**, *250* (21), 2811−2866.
(29) Mannix, A. J.; Zhou, X.-F.; Kiraly, B.; Wood, J. D.; Alducin, D.; Myers, B. D.; Liu, X.; Fisher, B. L.; Santiago, U.; Guest, J. R.; Yacaman, M. J.; Ponce, A.; Oganov, A. R.; Hersam, M. C.; Guisinger, N. P. Synthesis of borophenes: Anisotropic, two-dimensional boron polymorphs. *Science* **2015**, *350* (6267), 1513−1516.
(30) Feng, B.; Zhang, J.; Zhong, Q.; Li, W.; Li, S.; Li, H.; Cheng, P.; Meng, S.; Chen, L.; Wu, K. Experimental realization of two-dimensional boron sheets. *Nat. Chem.* **2016**, *8* (6), 563−568.
(31) Zhong, Q.; Zhang, J.; Cheng, P.; Feng, B.; Li, W.; Sheng, S.; Li, H.; Meng, S.; Chen, L.; Wu, K. Metastable phases of 2D boron sheets on Ag(111). *J. Phys.: Condens. Matter* **2017**, *29* (9), 095002.
(32) Liu, X.; Li, Q.; Ruan, Q.; Rahn, M. S.; Yakobson, B. I.; Hersam, M. C. Borophene synthesis beyond the single-atomic-layer limit. *Nat. Mater.* **2022**, *21* (1), 35−40.
(33) Wu, R.; Drozdov, I. K.; Eltinge, S.; Zahl, P.; Ismail-Beigi, S.; Bozovic, I.; Gozar, A. Large-area single-crystal sheets of borophene on Cu(111) surfaces. *Nat. Nanotechnol.* **2019**, *14* (1), 44−49.
(34) Li, H.; Yang, J.; Ma, Y.; Liu, G.; Xu, X.; Huo, Z.; Chen, J.; Li, J.; Zhang, W.; Wang, K.; Chen, L.; Xiao, X. Monolayer Borophene Formation on Cu(111) Surface Trigger ed by ⟨1$\bar{1}$0⟩ Step Edge. *Small* **2024**, *20* (7), No. e2303502.
(35) Chen, C.; Lv, H.; Zhang, P.; Zhuo, Z.; Wang, Y.; Ma, C.; Li, W.; Wang, X.; Feng, B.; Cheng, P.; Wu, X.; Wu, K.; Chen, L. Synthesis of bilayer borophene. *Nat. Chem.* **2022**, *14* (1), 25−31.
(36) Wu, R.; Eltinge, S.; Drozdov, I. K.; Gozar, A.; Zahl, P.; Sadowski, J. T.; Ismail-Beigi, S.; Bozovic, I. Micrometre-scale single-crystalline borophene on a square-lattice Cu(100) surface. *Nat. Chem.* **2022**, *14* (4), 377−383.
(37) Kiraly, B.; Liu, X.; Wang, L.; Zhang, Z.; Mannix, A. J.; Fisher, B. L.; Yakobson, B. I.; Hersam, M. C.; Guisinger, N. P. Borophene Synthesis on Au(111). *ACS Nano* **2019**, *13* (4), 3816−3822.
(38) Li, W.; Kong, L.; Chen, C.; Gou, J.; Sheng, S.; Zhang, W.; Li, H.; Chen, L.; Cheng, P.; Wu, K. Experimental realization of honeycomb borophene. *Sci. Bull.* **2018**, *63* (5), 282−286.
(39) Vinogradov, N. A.; Lyalin, A.; Taketsugu, T.; Vinogradov, A. S.; Preobrajenski, A. Single-Phase Borophene on Ir(111): Formation, Structure, and Decoupling from the Support. *ACS Nano* **2019**, *13* (12), 14511−14518.
(40) Zhang, L. Z.; Yan, Q. B.; Du, S. X.; Su, G.; Gao, H. J. Boron Sheet Adsorbed on Metal Surfaces: Structures and Electronic Properties. *J. Phys. Chem. C* **2012**, *116* (34), 18202−18206.
(41) Liu, Y.; Penev, E. S.; Yakobson, B. I. Probing the synthesis of two-dimensional boron by first-principles computations. *Angew. Chem., Int. Ed. Engl.* **2013**, *52* (11), 3156−3159.
(42) Zhang, Z.; Yang, Y.; Gao, G.; Yakobson, B. I. Two-Dimensional Boron Monolayers Mediated by Metal Substrates. *Angew. Chem., Int. Ed. Engl.* **2015**, *54* (44), 13022−13026.
(43) Tang, H.; Ismail-Beigi, S. Self-doping in boron sheets from first principles: A route to structural design of metal boride nanostructures. *Phys. Rev. B* **2009**, *80* (13), 134113.
(44) Pan, L.-L.; Li, J.; Wang, L.-S. Low-lying isomers of the B_9^- boron cluster: The planar molecular wheel versus three-dimensional structures. *J. Chem. Phys.* **2008**, *129* (2), 024302.
(45) Tai, T. B.; Grant, D. J.; Nguyen, M. T.; Dixon, D. A. Thermochemistry and Electronic Structure of Small Boron Clusters (B_n, n = 5−13) and Their Anions. *J. Phys. Chem. A* **2010**, *114* (2), 994−1007.
(46) Xu, C. Q.; Wang, T.; Wang, C.; Dong, X. R.; Zheng, H.; Zhao, Y.; Pan, L. L.; Yang, J.; Zhang, W.; Wu, G.; Xie, H.; Li, G.; Li, J.; Jiang, L.; Yang, X.; Wang, L. S. Observation of the Smallest Three-Dimensional Neutral Boron Cluster. *Angew. Chem., Int. Ed.* **2025**, *64* (8), No. e202419089.
(47) Blochl, P. E.; Margl, P.; Schwarz, K. Ab initio molecular dynamics with the projector augmented wave method. *Acs Sym. Ser.* **1996**, *629*, 54−69.
(48) Blochl, P. E. Projector Augmented-Wave Method. *Phys. Rev. B* **1994**, *50* (24), 17953−17979.
(49) Kresse, G.; Furthmuller, J. Efficiency of ab-initio total energy calculations for metals and semiconductors using a plane-wave basis set. *Comput. Mater. Sci.* **1996**, *6* (1), 15−50.
(50) Kresse, G.; Hafner, J. Ab-Initio Molecular-Dynamics Simulation of the Liquid-Metal Amorphous-Semiconductor Transition in Germanium. *Phys. Rev. B* **1994**, *49* (20), 14251−14269.

https://doi.org/10.1021/jacs.5c18362
J. Am. Chem. Soc. 2026, 148, 8276−8284

(51) Perdew, J. P.; Burke, K.; Ernzerhof, M. Generalized gradient approximation made simple. *Phys. Rev. Lett.* **1996**, *77* (18), 3865−3868.
(52) Henkelman, G.; Uberuaga, B. P.; Jónsson, H. A climbing image nudged elastic band method for finding saddle points and minimum energy paths. *J. Chem. Phys.* **2000**, *113* (22), 9901−9904.
(53) Tersoff, J.; Hamann, D. R. Theory of the scanning tunneling microscope. *Phys. Rev. B* **1985**, *31* (2), 805−813.
(54) Lee, C.; Yang, W. T.; Parr, R. G. Development of the Colle-Salvetti correlation-energy formula into a functional of the electron density. *Phys. Rev. B* **1988**, *37* (2), 785−789.
(55) Becke, A. D. Density-functional thermochemistry. III. The role of exact exchange. *J. Chem. Phys.* **1993**, *98* (7), 5648−5652.
(56) Stephens, P. J.; Devlin, F. J.; Chabalowski, C. F.; Frisch, M. J. Ab Initio Calculation of Vibrational Absorption and Circular Dichroism Spectra Using Density Functional Force Fields. *J. Phys. Chem.* **1994**, *98* (45), 11623−11627.
(57) Lu, T.; Chen, F. W. Multiwfn: A multifunctional wavefunction analyzer. *J. Comput. Chem.* **2012**, *33* (5), 580−592.

https://doi.org/10.1021/jacs.5c18362
J. Am. Chem. Soc. 2026, 148, 8276−8284